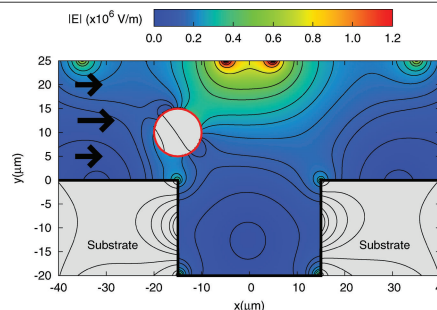




Numerical design of electrical-mechanical traps

Duc Vinh Le, Carlos Rosales, Boo Cheong Khoo* and Jaime Peraire

Effects of electrical and hydrodynamic forces on deformable cells are investigated in hybrid electrical-mechanical traps using the coupled IIM-BEM numerical technique. The technique makes useful quantitative predictions of the performance of different trap designs.



Please check this proof carefully. **Our staff will not read it in detail after you have returned it.**

Translation errors between word-processor files and typesetting systems can occur so the whole proof needs to be read. Please pay particular attention to: tabulated material; equations; numerical data; figures and graphics; and references. If you have not already indicated the corresponding author(s) please mark their name(s) with an asterisk. Please e-mail a list of corrections or the PDF with electronic notes attached – do not change the text within the PDF file or send a revised manuscript.

Please bear in mind that minor layout improvements, e.g. in line breaking, table widths and graphic placement, are routinely applied to the final version.

We will publish articles on the web as soon as possible after receiving your corrections; no late corrections will be made.

Please return your **final** corrections, where possible within **48 hours** of receipt by e-mail to: proofs@rsc.org

Reprints—Electronic (PDF) reprints will be provided free of charge to the corresponding author. Enquiries about purchasing paper reprints should be addressed via: <http://www.rsc.org/Publishing/ReSource/PaperReprints/>. Costs for reprints are below:

Reprint costs		
No of pages	Cost for 50 copies	Cost for additional 50 copies
2–4	£190	£120
5–8	£315	£230
9–20	£630	£500
21–40	£1155	£915
>40	£1785	£1525

Cost for including cover of journal issue:
£55 per 50 copies

Q1 Numerical design of electrical-mechanical traps†Duc Vinh Le,^a Carlos Rosales,^{b,c} Boo Cheong Khoo^{*a,c} and Jaime Peraire^{a,d}

Received 26th November 2007, Accepted 10th March 2008

First published as an Advance Article on the web ??????

DOI: 10.1039/b718153a

We present a coupled immersed interface method-boundary element method (IIM-BEM) numerical technique that predicts the behaviour of deformable cells under the effect of both hydrodynamic and electrical forces. This technique is applied to the study of a hybrid electrical-mechanical trap for single-cell trapping. We report on the effect of different combinations of electrode positions and mechanical properties of the trap on the maximum loading and unloading Reynolds numbers. We also report on the effect that cells moving with the flow have on cells which have been already trapped in a cavity.

Introduction

Individual cell trapping and manipulation is rapidly becoming one of the most useful tools in biomedical research.^{1–3} Creating large arrays of individual cell traps allows detailed statistical studies of cell responses to different treatments with a minimal consumption of reactants. The technology currently used to create arrays of single-cell traps is based on combinations of surface patterning, microfluidic design, and electrical fields.^{4,5}

Amongst the electrical techniques used to manipulate biological material, dielectrophoretic (DEP) traps show great promise, as they are highly sensitive to the electrical properties of cells—allowing for accurate cell separation^{6,7} and characterization^{8,9}—and have the ability to stably trap cells suspended in a liquid while avoiding all contact with the container walls.

Dielectrophoretic traps work by creating a non-homogeneous electrical field within the trap volume. As a cell enters the trap it is polarized by the external field; then the interaction between the electrical field gradient and the cell polarization produces a net force which is used to trap the cell. Depending on the dielectric properties of the liquid buffer and the cell, and on the frequency of the applied field, the DEP force can be positive (cells move towards the highest field region in the trap) or negative (cells move towards the electric field minimum in the trap).^{10,11} Although positive dielectrophoresis tends to produce stronger trapping fields, it has the severe disadvantage of moving the cells towards the electrode edges where the heat dissipation is highest and the cells may contact the container walls.¹² In most cases

these are characteristics to be avoided with living material, and for this reason we have chosen negative DEP cell traps to show the capabilities of our technique.

Although the use of hybrid electrical-mechanical devices to trap single cells has been demonstrated in experiments⁴ there are at present no systematic studies of their loading and unloading characteristics. The use of numerical methods is ideal for this purpose, as many different trap configurations can be studied in a controlled manner and in a relatively short period of time. However, as pointed out by Rosenthal *et al.*,¹³ the inclusion of both rigid and flexible boundaries in the numerical analysis of hybrid DEP-mechanical traps is a very difficult task. It is the purpose of this work to introduce the coupled IIM-BEM method as a flexible tool for the study of the complex phenomena that takes place in electrical-mechanical traps.

In our numerical studies, the immersed interface method (IIM) provides the means of calculating hydrodynamic effects and fluid-structure interaction effects such as cell deformation, and the boundary element method (BEM) is used to calculate the electric fields and their effects on the particle. The implementations of the IIM and the BEM used in this work have both been independently tested.^{14,15} By using both IIM and BEM techniques together, we can explore the behavior of target cells in detail, and describe the cell deformation and motion under the effects of both the electric and the flow fields. In addition, we can also analyze how a trapped cell behaves when it interacts with a second cell suspended in the fluid. This provides important information that is needed in order to ensure that a single-cell is trapped per trapping site in an array instead of two or more.

This paper is divided into four main sections. Section two describes the IIM and the BEM techniques, section three describes a study of a two-dimensional single-cell trap that uses both mechanical and dielectrophoretic trapping for maximum effect, and finally, section four contains the discussion of our results.

Materials and methods

Governing equations. The application we consider includes a viscous flow problem and an electrostatic problem as shown in Fig. 1. For the viscous flow problem, we consider the

^aSingapore-MIT Alliance, E4-04-10, 4 Engineering Drive, Singapore 117576. E-mail: smaldv@nus.edu.sg

^bInstitute of High Performance Computing, 1 Science Park Road, #01-01 The Capricorn, Singapore 117528. E-mail: carlos@ihpc.a-star.edu.sg

^cDepartment of Mechanical Engineering, National University of Singapore, Kent Ridge Crescent, Singapore 119260.

E-mail: mpekbc@nus.edu.sg; Fax: +6567791459; Tel: +6568742889

^dDepartment of Aeronautics and Astronautics, Massachusetts Institute of Technology, 77 Massachusetts Ave, Cambridge, MA, 02139, USA. E-mail: peraire@mit.edu

† Electronic supplementary information (ESI) available: Two movie files showing the interaction between a trapped particle and a second particle moving downstream. See DOI: 10.1039/b718153a

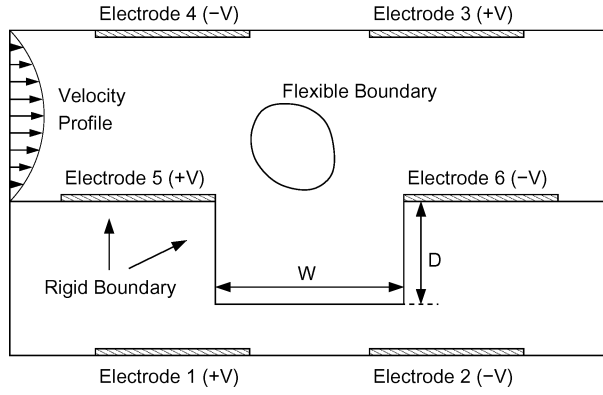


Fig. 1 A typical domain in which the Navier–Stokes equations and electrostatic problems are solved. See main text for the different electrode combinations used.

incompressible Navier–Stokes equations formulated in primitive variables, written as

$$\rho(\mathbf{u}_t + (\mathbf{u} \cdot \nabla)\mathbf{u}) + \nabla p = \mu \Delta \mathbf{u} + \mathbf{F} \quad (1)$$

$$\nabla \cdot \mathbf{u} = 0 \quad (2)$$

5 with boundary conditions

$$\mathbf{u}|_{\partial\Omega} = \mathbf{u}_b \quad (3)$$

where \mathbf{u} is the fluid velocity, p is the pressure, ρ is the density, and μ the viscosity of the fluid. Throughout this paper, we assume that the fluid density ρ and the viscosity μ are constant over the whole domain. The Navier–Stokes equations are considered in a 2-dimensional bounded domain Ω that contains rigid boundaries and deformable material interfaces $\Gamma(t)$. The effect of the material interface $\Gamma(t)$ immersed in the fluid results in a singular force \mathbf{F} which has the form

$$\mathbf{F}(\mathbf{x}, t) = \int_{\Gamma(t)} \mathbf{f}(s, t) \delta(\mathbf{x} - \mathbf{X}(s, t)) ds, \quad (4)$$

where $\mathbf{X}(s, t)$ is the arc-length parametrization of $\Gamma(t)$, s is the arc-length, $\mathbf{x} = (x, y)$ is spatial position, and $\mathbf{f}(s, t)$ is the force strength. Here, $\delta(\mathbf{x})$ is the two-dimensional Dirac function. The motion of the interfaces satisfies

$$\frac{\partial}{\partial t} \mathbf{X}(s, t) = \mathbf{u}(\mathbf{X}, t) = \int_{\Omega} \mathbf{u}(\mathbf{x}, t) \delta(\mathbf{x} - \mathbf{X}(s, t)) d\mathbf{x}. \quad (5)$$

The strength of the singular forces at the rigid boundaries is determined by solving a small system of equations at each timestep to impose the no-slip conditions at the rigid boundaries.

10 The forces that the deformable boundary exerts on the fluid are the elastic force and the dielectrophoretic force, which are applied to the fluid through the jump conditions,

$$\mathbf{f}(s, t) = \mathbf{f}^{\text{elastic}}(s, t) + \mathbf{f}^{\text{DEP}}(s, t) \quad (6)$$

The elastic force, $\mathbf{f}^{\text{elastic}}(s, t)$, exerted by the immersed boundary on the fluid is given as

$$\mathbf{f}^{\text{elastic}}(s, t) = \frac{\partial}{\partial s} (T(s, t) \boldsymbol{\tau}(s, t)), \quad (7)$$

where $T(s, t)$ is defined as

$$T(s, t) = T_0 \left(\left| \frac{\partial \mathbf{X}(s, t)}{\partial s_0} \right| - 1 \right) \quad (8)$$

and $\boldsymbol{\tau}(s, t)$ is the unit tangential vector to the interface,

$$\boldsymbol{\tau}(s, t) = \frac{\partial \mathbf{X}}{\partial s} \bigg/ \left| \frac{\partial \mathbf{X}}{\partial s} \right| \quad (9)$$

Here, s and s_0 are the arc-lengths measured along the current and undeformed configuration of the interface, respectively. The scalar T_0 is the stiffness constant which describes the elastic property of the flexible boundary. 15

The DEP force, $\mathbf{f}^{\text{DEP}}(s, t)$, is calculated by solving an electrostatic problem in a system with conductors (the electrodes) and piecewise homogeneous dielectrics (the fluid, the particle and the substrate). Assuming neutrally charged particles this problem is governed by Laplace's equation within each of the material subdomains: 20

$$\nabla^2 \phi = 0 \quad (10)$$

The boundary conditions applied are given potential values at the electrodes and continuity of the potential and the normal component of the electric displacement at every material interface: 25

$$\phi(x) = \phi_0 \text{ if } x \in \text{electrode surface} \quad (11)$$

$$\left. \begin{aligned} \phi_1(x) &= \phi_2(x) \\ \tilde{\epsilon}_1 \frac{\partial \phi_1}{\partial n} \bigg|_x &= \tilde{\epsilon}_2 \frac{\partial \phi_2}{\partial n} \bigg|_x \end{aligned} \right\} \text{ if } x \in \text{interface} \quad (12)$$

where $\tilde{\epsilon}_i = \epsilon_i - j\sigma_i/\omega$ is the complex permittivity of material i ; ϵ_i and σ_i are the dielectric permittivity and the electric conductivity of medium i ; j is $\sqrt{-1}$ and ω is the radial frequency of the external field. 30

The electric field is calculated as the negative of the gradient of the potential: 35

$$\mathbf{E} = -\nabla \phi \quad (13)$$

The total force acting on a suspended particle can be calculated using the Maxwell stress tensor method, where the total force is calculated as the integrated stress tensor \mathbf{T}_M over the surface Γ of the particle:

$$\mathbf{F}(t)_{\text{DEP}} = \oint (\mathbf{T}_M \cdot \mathbf{n}) d\Gamma \quad (14)$$

where \mathbf{n} is the unit vector normal to the surface and t is time. In most DEP studies the electric field has a frequency below 100 MHz and, therefore, a wavelength that is at least a few metres long. This is several orders of magnitude larger than the dimensions of typical electrode structures in DEP devices and thus the near-field approximation can be used and effects due to magnetic field components neglected.¹⁶ In this approximation the Maxwell stress tensor for a general, conductive dielectric medium, is given by:

$$\mathbf{T}_M = \epsilon \left(\mathbf{E}\mathbf{E} - \frac{1}{2} \mathbf{E}^2 \mathbf{I} \right) \quad (15)$$

This is regarded as the most rigorous approach to derive field-induced forces. For an applied harmonic electrical field the time-averaged net DEP force on a particle using this method is given as:¹⁶

$$\langle \mathbf{F}_{\text{DEP}}(t) \rangle = \frac{\epsilon_t}{4} \oint \{ [(\mathbf{E}_t \mathbf{E}_t^* + \mathbf{E}_t^* \mathbf{E}_t) - |\mathbf{E}_t|^2 \mathbf{I}] \cdot \mathbf{n} \} d\Gamma \quad (16)$$

Here, $E_i E_i^*$ is the diadic product of the electric field and its complex conjugate, and the subscript f indicates quantities corresponding to the fluid medium where the particle is suspended. The dependence in time t is kept because as the particle moves the average DEP force will change due to the different electric field distribution. Notice that this approximation will only be valid as long as the frequency of the externally applied field is much higher than the velocity at which changes in position of the particle occur. Let the particle velocity divided by the particle size, $f_{\text{move}} = u_p/d_p$, define a frequency associated to the particle movement. Typical frequencies of DEP traps belong in the MHz range, taking a typical cell of diameter of 10 μm and a typical velocity of cell transport in microchannels of 1 mm/s we find that:

$$\frac{f_{\text{field}}}{f_{\text{move}}} \approx \frac{10^6}{(10^{-3}/10^{-5})} = 10^4 \gg 1 \quad (17)$$

which certainly allows us to use the average DEP force as described above.

To couple efficiently this force calculation to the IIM, we must provide the force density at the interface, as given by the differential form of eqn (16):

$$\langle \mathbf{F}_{\text{DEP}}(t) \rangle = \frac{\epsilon_f}{4} [(\mathbf{E}_f \mathbf{E}_f^* + \mathbf{E}_f^* \mathbf{E}_f) - |\mathbf{E}_f|^2 \mathbf{I}] \cdot \mathbf{n} \quad (18)$$

The IIM and the BEM complement each other because the BEM can provide the electrical force at any point in the surface of a suspended cell, and the IIM requires this force to predict the level of deformation and movement of the cell in each time step of the simulation. On the other hand, the BEM solver takes as input the new position and shape of the interface provided by the IIM and produces new values of the force which are then fed back to the IIM solver. The coupled system is solved using a semi-implicit time integration scheme and this procedure is repeated continuously.

Electric field calculation using BEM. The indirect formulation of the BEM^{17,18} with only sources has been chosen because its implementation for systems with multiple material interfaces is simpler than the corresponding implementation for the direct formulation. In this technique, the interfaces separating two dielectric materials are represented by equivalent polarization charge densities, and the interfaces separating a dielectric from a conductor are represented by a total charge density that is the sum of the free charge of the conductor and the polarization charge of the dielectric.

The interfaces in the problem are discretized using isoparametric quadratic line elements, and using the collocation method a system of linear equations describing the electrical problem is obtained.

The equations for a system with $i = 1, \dots, Ne$ nodes in the electrodes, $i = Ne + 1, \dots, N$ nodes in the dielectric interfaces, and a total of NE elements in the discretized surfaces are:

$$\phi_i = \frac{1}{2\pi\epsilon_0} \sum_j \sum_k \rho_{s,jk} \int_{\Gamma_j} M_{jk}(\mathbf{r}') \ln \frac{1}{|\mathbf{r} - \mathbf{r}'|} d\Gamma', \quad i = 1, \dots, Ne \quad (19)$$

$$\rho_{s,i} = \frac{\tilde{\epsilon}_c - \tilde{\epsilon}_i}{2\pi(\tilde{\epsilon}_c + \tilde{\epsilon}_i)} \sum_j \sum_k \rho_{s,jk} \int_{\Gamma_j} M_{jk}(\mathbf{r}') \frac{(\mathbf{r} - \mathbf{r}') \cdot \hat{\mathbf{n}}}{|\mathbf{r} - \mathbf{r}'|^2} d\Gamma', \quad i = Ne + 1, \dots, N. \quad (20)$$

In these equations ϕ_i and $\rho_{s,i}$ stand for the potential and the charge density at node i , $\rho_{s,jk}$ is the charge density at node k of element j , and M_{jk} is the k th shape function in element j . This yields a dense matrix system that must be solved for $\rho_{s,i}$.

The linear system is solved using the GMRES iterative method¹⁹ with a simple Jacobi preconditioner.²⁰ The first timestep is solved using a zero guess for the solution vector. Subsequent solutions use the solution vector from previous timestep as the initial guess for the solver; this greatly reduces the solution time.

Once the solution to the equations is found, the electric field at any point in the domain can be obtained by using the expression $\mathbf{E} = -\nabla\phi$ where the derivatives of the potential are taken directly over eqn (19):

$$E_i = \frac{1}{2\pi\epsilon_0} \sum_j \sum_k \rho_{s,jk} \int_{\Gamma_j} M_{jk}(\mathbf{r}') \frac{(\mathbf{r} - \mathbf{r}') \cdot \hat{\mathbf{i}}}{|\mathbf{r} - \mathbf{r}'|^2} d\Gamma', \quad i = x, y, z \quad (21)$$

Viscous flow calculation using IIM. The immersed interface method is employed to solve the Navier–Stokes equations by using the finite difference method on a staggered Cartesian grid. The IIM was originally proposed by LeVeque and Li^{21,22} for solving elliptic equations and Stokes flow. The method was developed further for the Navier–Stokes equations.^{23–25} The IIM was also used for solving the two-dimensional streamfunction–vorticity equations on irregular domains.^{26–28} Recently, the IIM has been developed to handle rigid and flexible boundaries simultaneously.¹⁴

Our IIM for solving viscous flow problem is largely based on that described in Le *et al.*¹⁴ The singular forces along the cell interfaces are the elastic and dielectrophoretic forces, which are computed based on the configuration of the interfaces. The DEP force is calculated by solving an electrostatic problem using the BEM technique. BEM is a natural choice for solving the electrostatic problem because the only quantity that we are interested in is the DEP force acting along the cell boundary. The singular force at the rigid boundary is determined by imposing the no-slip condition. Once all the singular forces have been computed, the jump in pressure and jumps in the derivatives of both pressure and velocity are calculated and incorporated into the finite difference discretization to obtain a sharp interface resolution.

Our numerical algorithm is based on the pressure-increment projection algorithm for the discretization of the Navier–Stokes equations with special treatment at the grid points near the interface.¹⁴ The spatial discretization is carried out on a standard marker-and-cell (MAC) staggered grid similar to that found in Kim and Moin.²⁹ Given the velocity \mathbf{u}^n , the pressure $p^{n-1/2}$, and the singular forces $\mathbf{f}^n, \mathbf{f}^{n+1}$, we compute the

velocity \mathbf{u}^{n+1} and pressure $p^{n+1/2}$ at the next time step as follows:
Step 1: Compute an intermediate velocity field \mathbf{u}^* by solving

$$\frac{\mathbf{u}^* - \mathbf{u}^n}{\Delta t} = -(\mathbf{u}\nabla\mathbf{u})^{n+\frac{1}{2}} - \frac{1}{\rho}\nabla p^{n+\frac{1}{2}} + \frac{\mu}{2\rho}(\nabla_h^2\mathbf{u}^* + \nabla_h^2\mathbf{u}^n) + \mathbf{C}_1 \quad (22)$$

$$\mathbf{u}^*|_{\partial\Omega} = \mathbf{u}_b$$

where the advective term is extrapolated using the formula,

$$(\mathbf{u}\nabla\mathbf{u})^{n+\frac{1}{2}} = \frac{3}{2}(\mathbf{u}\nabla_h\mathbf{u})^n - \frac{1}{2}(\mathbf{u}\nabla_h\mathbf{u})^{n-1} + \mathbf{C}_2 + \gamma_1[\mathbf{u}\nabla\mathbf{u}]_t \quad (23)$$

and the pressure gradient is approximated simply as,

$$\nabla p^{n+\frac{1}{2}} = G^{\text{MAC}}p^{n-\frac{1}{2}} + \mathbf{C}_3 + \gamma_2[\nabla p]_t \quad (24)$$

Step 2: Compute a pressure increment ψ^{n+1} and update pressure and velocity field

$$\nabla_h^2\psi^{n+1} = \rho\frac{D^{\text{MAC}}\mathbf{u}^*}{\Delta t} + \mathbf{C}_4, \quad \mathbf{n}\nabla\psi^{n+1}|_{\partial\Omega} = 0, \quad (25)$$

$$\mathbf{u}^{n+1} = \mathbf{u}^* - \frac{1}{\rho}\Delta t G^{\text{MAC}}\psi^{n+1} + \mathbf{C}_5, \quad (26)$$

$$p^{n+1/2} = p^{n-1/2} + \psi^{n+1} - \frac{\mu}{2\rho}(D^{\text{MAC}}\mathbf{u}^*) + C_6 \quad (27)$$

We note that the above projection method is analogous to the pressure-increment projection method³⁰ at most of the grid points except at some grid points near the interface. The discretization of the Navier–Stokes equations at those grid points near the interface needs to be modified to account for the jump conditions across the interface due to the presence of singular forces at the interface. The coefficients C_i , $i = 1, \dots, 6$, are the spatial correction terms added to the finite difference equations at the points near the interface to improve the accuracy of the local finite difference approximations. These correction terms can be computed by using the generalized finite difference formulas^{14,31} if we know the jumps in the solution and their derivatives. The explicit form of the coefficients C_i , $i = 1, \dots, 6$ can be found in Le *et al.*¹⁴ In addition to the spatial correction terms, we also need to perform corrections for the jump in time. The term $[\cdot]_t$ in eqns (23) and (24) denotes a jump in time and is only non zero when the interface crosses the grid point over the time interval considered. The coefficients γ_1 and γ_2 correspond to the first order corrections in time.¹⁴ In the above expressions, ∇_h and ∇_h^2 are the standard central difference operators, G^{MAC} and D^{MAC} are the MAC gradient and divergence operators, respectively.¹⁴

In our projection method, we need to solve, at each timestep, two Helmholtz equations for \mathbf{u}^* in eqn (22) and one Poisson equation for ψ^{n+1} in eqn (25). Since the correction terms in eqns (22) and (25) only affect the right-hand sides of the discrete systems for the Helmholtz and Poisson equations, we can take advantage of the fast solvers from FISHPACK³² to solve these equations.

Results

In this section we present a validation study of the numerical methodology followed by the detailed analysis of three different electrode configurations for the fixed geometry shown in Fig. 1

and the effect of changes in the geometry for the most efficient of the three electrode configurations. After this analysis, we also present a series of simulations which assess the effect of having more than a single particle in the trapping area.

Model validation

In this section we compare numerical predictions from our model with previously published experimental results by Dürr *et al.*,³³ where the threshold velocity of latex beads was measured as a function of the applied potential at the electrodes.

Dürr *et al.* considered pairs of electrodes situated opposite to one another in the top and bottom walls of a microchannel. Each electrode pair is equivalent to a parallel plate capacitor, and in this configuration the electrical field gradient at the ends of the electrodes generates the necessary DEP force to stop or deviate the particles moving along the microchannel.

We focus on one of the measurements reported by Dürr *et al.*, the threshold velocity for a latex sphere of diameter 2 μm as a function of the potential difference between a pair of electrodes of width 20 μm in a channel of height 25 μm . This case is adequate for comparison with our 2D model because the electrodes used in the experiment are very long in comparison with their width (4.85 mm in length vs. 20 μm in width) and so end effects in the direction normal to the flow are negligible.

The buffer suspension conductivity for both the experiments and our numerical calculations was $\sigma_f = 0.06 \text{ S m}^{-1}$, and its dielectric permittivity $\epsilon_f = 80$, and the frequency of the applied field 2.0 MHz. The values reported by Dürr *et al.* for the conductivity and permittivity of the latex particles, $\sigma_p = 0 \text{ S m}^{-1}$ and $\epsilon_p = 3.5$, were also used in the simulation without modification.

The numerical predictions from our model are close to the experimental results, as shown in Fig. 2, but the threshold velocity is consistently underestimated at high potential values. After careful consideration we concluded that this deviation was due to ignoring of the thermal effects in the numerical calculation. At high values of the applied potential the temperature of the liquid will increase due to Joule heating,³⁴ producing a reduction in the viscosity and therefore reducing the force that the liquid

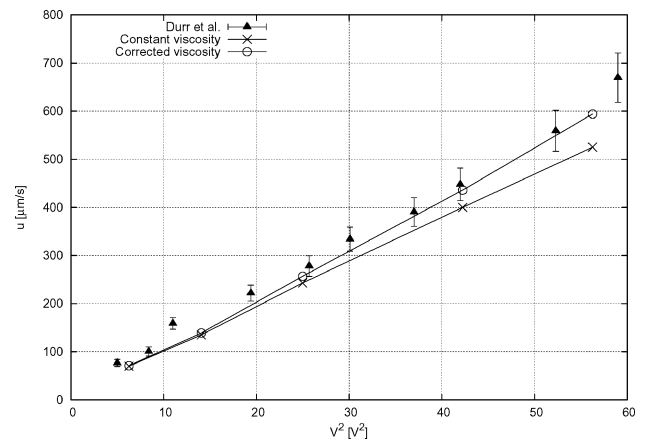


Fig. 2 Comparison of predicted holding velocities and experimental values reported by Dürr *et al.*³³ Excellent agreement between numerical and experimental values is found when considering the temperature induced change in the liquid viscosity.

exerts on the particle. An approximate equation describing the temperature increase in the liquid due to the electric field in DEP traps was given³⁵ as $\nabla^2(\nabla T) = -\sigma|E|^2/\kappa$ where σ and κ are the electric and thermal conductivity of the liquid and E is the electric field. An order of magnitude calculation gives:

$$\frac{\Delta T}{\Delta x^2} \approx \frac{\sigma}{\kappa} |E|^2 \approx \frac{\sigma}{\kappa} \left(\frac{V}{\Delta x}\right)^2 \quad (28)$$

This yields the simple expression $\Delta T \approx \sigma V^2/\kappa$. Using $\sigma = 0.06 \text{ S m}^{-1}$ as in the measurements made by Dürri *et al.* and $\kappa = 0.6 \text{ J ms}^{-1} \text{ K}^{-1}$ as the thermal conductivity of water, we obtain $\Delta T \approx 0.1 V^2$

5 We consider a variation of the viscosity with temperature of the form used by Petersen *et al.*,³⁶ $\mu(T) = 2.761 \times 10^{-6} \exp(1713/T)$ For a temperature increase ΔT in the fluid, and assuming that the fluid force exerted on the particle is proportional to the fluid viscosity, we can correct our calculations for the threshold velocity v using:

$$v_{\text{corrected}}(U, T) = v(U)cf(T, \Delta T) \quad (29)$$

where U is the applied potential and the correction factor cf is given by:

$$cf(T, \Delta T) = \frac{\mu(T)}{\mu(T + \Delta T)} = \frac{\exp\left(\frac{1713}{T}\right)}{\exp\left(\frac{1713}{T + \Delta T}\right)} \quad (30)$$

15 Once this viscosity correction is taken into account our calculations agree very well with the measured values of the threshold velocity across the full range of potential values as shown in Fig. 2.

Numerical analysis of trap design

Our first objective was to investigate the effect of adding a dielectrophoretic trapping force to a simple mechanical trap for different Reynolds numbers. We chose a fixed trap geometry, in which the physical well had a depth $D = 20 \mu\text{m}$ and a width $W = 30 \mu\text{m}$, and three different electrode configurations.

The different electrode configurations can be described by referring to Fig. 1. In electrode configuration 1 (EC-1) electrodes one to four are active, in electrode configuration 2 (EC-2) electrodes three to six are active, and in electrode configuration 3 (EC-3), only electrodes five and six are active. The electric field generated by each of the three electrode configurations when the particle is outside the cavity is shown in Fig. 3. The electric field minimum in these figures would correspond to the particle trapping location in the absence of hydrodynamics forces. For EC-1 the particle would be trapped inside the physical well, while for EC-2 the particle could be trapped either in the center of the channel, hovering over the physical well, or inside the well. The two minima of the electric field in EC-2 are separated by a field bottleneck that makes the movement from one of the minima to the other difficult. In EC-3 the situation is not as clear as for the other two configurations. It appears, however, that in this case the particle could be trapped either near the top of the channel or inside the well depending on the initial conditions.

40 The particle studied had a diameter of $10 \mu\text{m}$, stiffness constant $T_0 = 1 \text{ dyne cm}^{-1}$, and its conductivity and permittivity were $\sigma_p = 2 \times 10^{-3} \text{ S m}^{-1}$ and $\epsilon_p = 2.5$, respectively. The stiffness value chosen corresponds to that reported for a typical

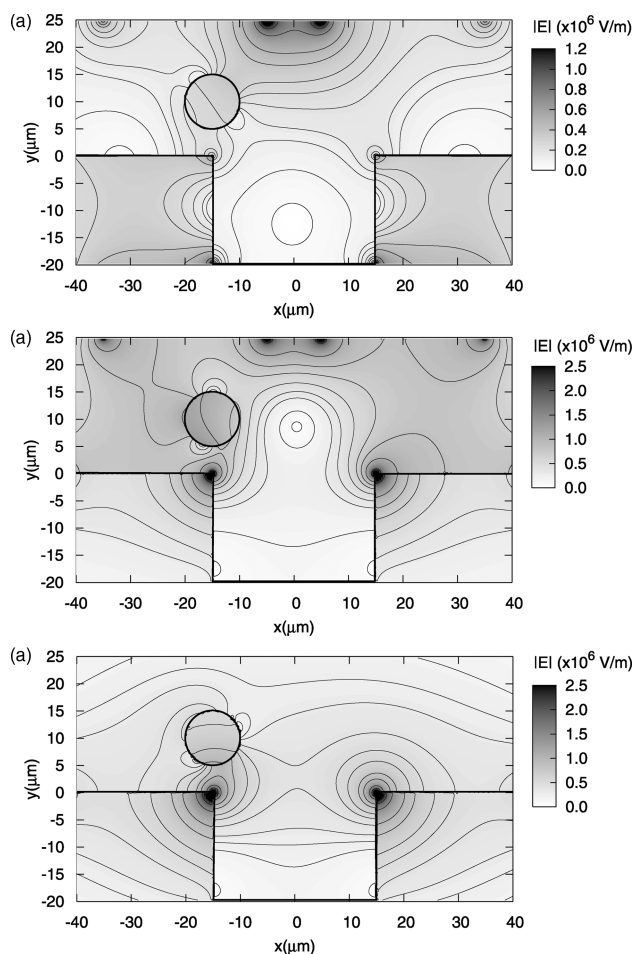
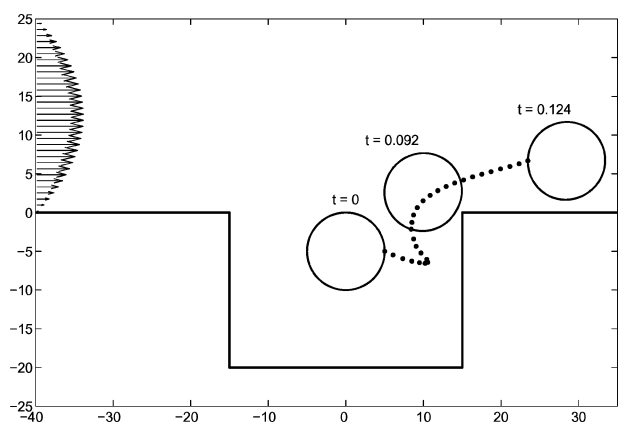


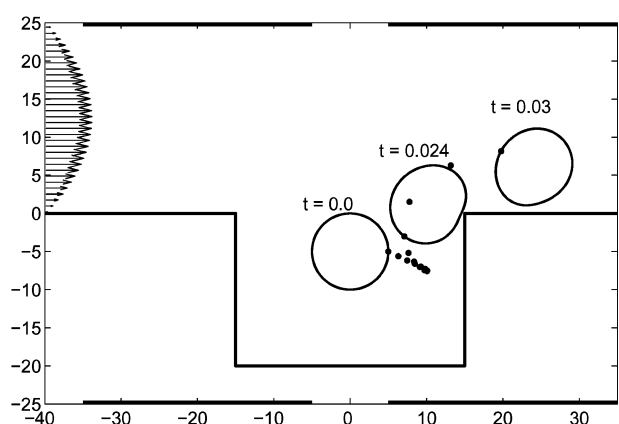
Fig. 3 Electric field for the three different electrode configurations of (a) EC-1, (b) EC-2 and (c) EC-3. Notice how the presence of the particle alters the field distribution within the traps.

lipid bilayer.³⁷ This value is similar to those of endothelial cells and chondrocytes. Healthy erythrocytes and other blood cells are typically softer, with stiffness values on the order of $10^{-2} \text{ dyne cm}^{-1}$,³⁸ but their stiffness can increase dramatically due to sickness. The fluid buffer was assumed to be water with $\sigma_f = 10^{-4} \text{ S m}^{-1}$ and $\epsilon_f = 80$. The substrate was taken to be an insulating material with $\sigma_s = 0 \text{ S m}^{-1}$ and $\epsilon_s = 2.0$. The frequency of the applied potential is 1 MHz in all cases, which leads to negative dielectrophoresis in the region of maximum strength for the chosen materials. It is assumed that the cell and the fluid buffer have the same density $\rho = 10^3 \text{ kg m}^{-3}$ and viscosity $\mu = 10^{-3} \text{ kg ms}^{-1}$. In all our simulations, a parabolic velocity profile with maximum velocity U_{max} is prescribed at the inlet boundary. This U_{max} is varied to change the Reynolds number, $Re = \rho U_{\text{max}} L/\mu$ where L is the height of the channel which has the value of $25 \mu\text{m}$ in all examples.

Our first test was to assume that a particle was initially trapped in the center of the physical well and then run several simulations where the flow rate was progressively increased until the particle moved out of the cavity. We found that while a purely mechanical trap (with no active electrodes) released the particle for flow speeds above $U_{\text{max}} = 1.0 \text{ mm s}^{-1}$ ($Re = 0.025$) as shown in Fig. 4(a), all three electrode designs kept the particle trapped



(a)



(b)

Fig. 4 Trajectory of the particle in the trap with: (a) pure mechanical trap releases the particle at $U_{\max} = 1 \text{ mm s}^{-1}$, (b) electrode configuration 1 (EC-1) holds the particle trapped until $U_{\max} = 5 \text{ mm s}^{-1}$ ($Re = 0.125$). Solid dots correspond to the same control point on the boundary at different times.

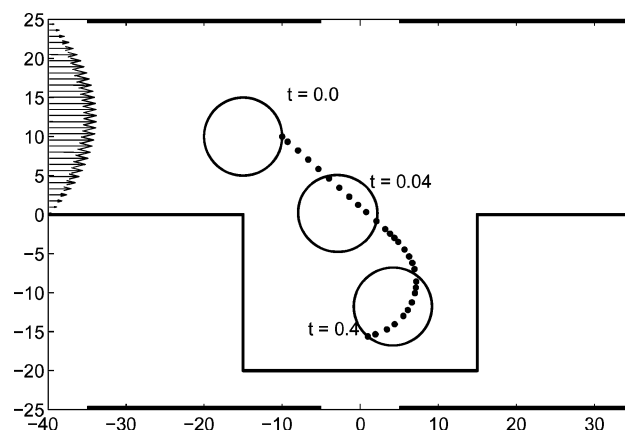
within the cavity beyond this value, although they also released the particle once the flow speed was sufficiently increased.

Our simulations indicate that both configurations EC-2 and EC-3 provide much stronger trapping than EC-1, and that EC-3 is the strongest configuration of the three. This can be attributed to the strong gradient generated at the edges of electrodes 5 and 6 (Fig. 1) which are only active in configurations EC-2 and EC-3. At flow speeds above 5.0 mm s^{-1} ($Re = 0.125$), electrode configuration 1 allows the particle to leave the cavity as shown in Fig. 4(b), while electrode configurations 2 and 3 keep the particle trapped. Electrode configuration 3 keeps the particle trapped at flow speeds as high as of 10 mm s^{-1} ($Re = 0.25$), an order of magnitude higher than the pure mechanical trap.

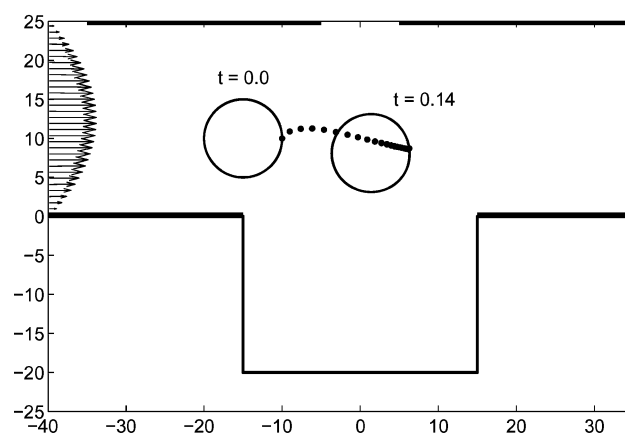
Although EC-3 gives the best configuration to use once the particle has been trapped, if the trap cannot capture passing particles, then its strength once it has been loaded, is meaningless for a trapping device designed to work in a continuous mode. In order to evaluate the effect of the three electrode configurations on the loading characteristics of the trap, we released a particle upstream of the trap—initial position as shown in Fig. 3—and

tracked its movement until it was stopped in an equilibrium position or moved beyond the physical well region.

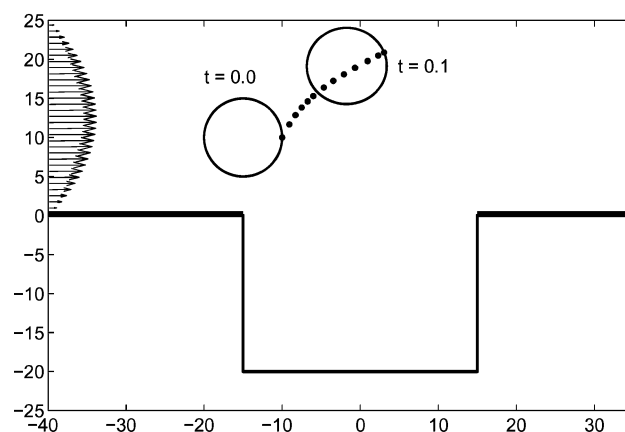
From the trajectories shown in Fig. 5, it is clear that only configuration 1 of the electrodes can possibly trap a particle originally placed outside the cavity inside the physical well.



(a)



(b)



(c)

Fig. 5 Trajectory of the particle in the trap. (a) EC-1 at $U_{\max} = 0.5 \text{ mm s}^{-1}$ ($Re = 0.0125$), (b) EC-2 at $U_{\max} = 0.2 \text{ mm s}^{-1}$ ($Re = 0.005$), (c) EC-3 at $U_{\max} = 0.2 \text{ mm s}^{-1}$ ($Re = 0.005$). No trapping occurred for the purely mechanical trap for this initial position of the particle, even for extremely low Reynolds numbers.

For all the three cases, the particle stops at a minimum of the electrical field, which is expected of a particle experiencing negative dielectrophoresis. However, neither electrode configuration 2 nor configuration 3 cause the particle to traverse towards the physical well, and therefore are not suitable for loading hybrid DEP traps. Notice that the particle is only trapped in configuration EC-2 (outside the cavity, as shown in Fig. 5(b)) for very low flow rates ($U_{\max} = 0.2 \text{ mm s}^{-1}$, or $Re = 0.005$) as compared to those in EC-1 (Fig. 5(a)).

In view of these results we next focused our studies on electrode configuration 1 since, although it does not provide the strongest trapping once the trap is loaded, it is the only configuration that enhances both the trapping strength and the loading efficiency of a purely mechanical trap. It is possible to design a trap with selectively activated electrodes to initially utilize EC-1 to move the particle into the cavity, and then switch to EC-3 to keep the particle trapped under higher flow rates. This requires identifying accurately the entry of the article into the cavity, and will be the subject of future work.

Trapping single-cell

Using electrode configuration 1, we studied the effect of varying the height and width of the physical well. In particular, we studied how the trap width and depth affected the loading and strength characteristics of the trap. For all the tests the initial position of the particle is outside the cavity as shown in Fig. 3.

Effect of the mechanical trap depth

Intuitively, the depth of the well should be important for trapping strength, as it should be much easier to remove a particle from a shallow trap than from a deep trap. But we expect that, eventually, the trap depth should reach a value where increasing it further has no effect on the trapping strength, as the particle will not have time to move downwards into the regions of the well which are isolated from the bulk flow. In order to test this idea, we fixed the trap width at $W = 30 \mu\text{m}$ and changed the depth of the well to study how the trapping strength was affected. For each depth, we then ran simulations with increasingly high Reynolds numbers and tracked the particle movement through the complete process of loading/unloading. We determined the critical Reynolds number Re_c for each value of the depth as that Re for which the particle could no longer be trapped inside the mechanical well due to the hydrodynamic forces. This corresponds to the critical Reynolds number for loading.

The results in Fig. 6(a) show precisely this behavior. In this case, after the well has reached a depth equal to 1.5 times the particle diameter increasing it further has no effect on the critical Reynolds number and therefore, the trapping strength. It is important to note that, even though this would be the expected behavior of the particle, without an efficient numerical method as presented in this work it would not be feasible to calculate quantitatively the optimal depth for a DEP hybrid trap.

Effect of the mechanical trap width

The width of a physical well has a very strong effect in the loading characteristics of the trap. If the physical well is too narrow it

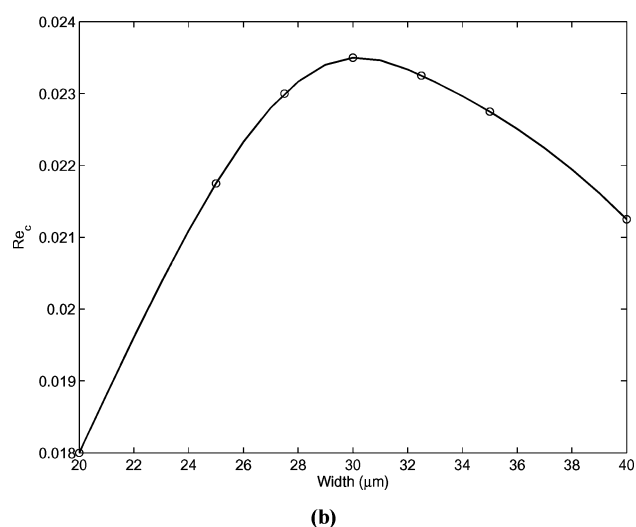
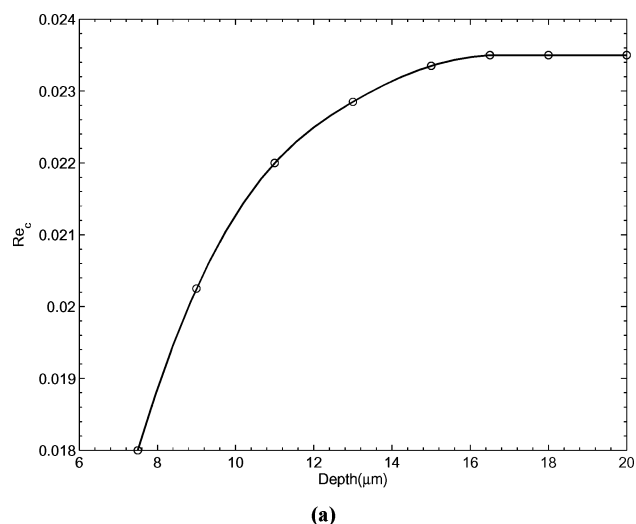


Fig. 6 Effect of cavity depth (a) and width (b) on the critical Reynolds number for a particle initially situated outside of the cavity as shown in Fig. 3. Notice the existence of an optimal width for the trap.

will be very difficult to trap the particle as the liquid velocity increases. On the other hand, if it is too wide the particle will simply skim over the well and move off without being trapped. In order to study this behavior we fixed the trap depth to $D = 15 \mu\text{m}$, which lies in the region where trapping strength is not affected by the trap depth, and changed the width of the well to see how it affected the critical Reynolds number.

Fig. 6(b) shows that narrow traps are weak and that the critical Reynolds number increases until it reaches a maximum for a width value equal to three times the particle size. After this maximum value is reached the critical Reynolds number decreases again, indicating that the trap becomes less effective.

Trapping multiple-cells

To show the flexibility of our technique, we present the results of the interaction between a trapped particle and a second particle moving downstream for two different positions of the trapped particle. The study was done for a fixed geometry with a physical well of depth $15 \mu\text{m}$ and width $30 \mu\text{m}$ with electrode configuration 1 and a maximum flow speed

$U_{\max} = 0.8 \text{ mm s}^{-1}$ ($Re = 0.02$). Both particles have identical mechanical and electrical properties.

Movie 1 (Electronic Supplementary Information†) shows the effect that a trapped particle has on other particles in the channel. When the trapped particle is at the center of the physical well (left column) the second particle is not trapped, but rather rolls over the already trapped particle and continues its downstream path. The second particle initially pushes the trapped particle, then rolls over it and collides with the edge of the well ($t = 0.08$) and continues its downstream path ($t = 0.14$) without being trapped.

When the trapped particle is closer to the leading edge of the physical well—Movie 2—the second particle is trapped. The initial steps are similar to those in the previous case, with the second particle pushing the trapped particle forward, then rolling over it, but when it comes into contact with the edge of the physical well it starts moving downwards ($t = 0.20$) and is eventually trapped ($t = 1.60$). In both examples, the particle interaction is shown to produce a rotation. This is due to the faster flow on the outside of the well, which produces a net torque on the particles and induces a rotational movement.

Similar differences in behavior can also be obtained by keeping the trapped particle at a constant initial position but changing the position of the electrodes and the dimensions of the well. These simulations show that small differences in the traps can lead to single- or multiple-cell trapping. Numerical simulations are ideally suited to produce controlled studies of single-cell traps, as dynamical behavior of the trap can be studied for controlled changes in all relevant parameters. Future studies using numerical tools should focus on the analysis of issues of practical relevance in cell trapping and separation, such as the effect of polydisperse size distributions on the behaviour and performance of the traps.

Conclusions

We have presented the coupled immersed interface method-boundary element method numerical technique for the solution of problems involving electrostatic and fluid forces on deformable bodies. We have shown the flexibility of the technique by applying it to the realistic problem of single-cell dielectrophoretic trap design.

We have found that, for the geometry used, there is an optimal width of the mechanical trap that allows maximum loading and trapping efficiency, and that beyond a certain value the depth of the well does not influence the trapping strength.

These are significant findings that highlight the relevance of simulation techniques in the design of biological cell traps. Quantitative tools like the IIM-BEM technique can be used to optimize current device designs and to provide insight into the development of future designs. More importantly, the use of these tools can shorten the production cycle of new devices.

The IIM-BEM technique was also applied to the analysis of multiple particle interaction in dielectrophoretic traps. As shown in the text, what we initially designed as a single-cell trap could turn into a multi-cell trap under certain circumstances. This influence of minor changes in the performance of single-cell dielectrophoretic traps indicates that detailed studies of the

loading and unloading of DEP traps are needed in order to guarantee the desired mode of operation.

Numerical methods are the ideal tools to do these detailed studies, as all relevant parameters can be changed in a controlled manner, and their effect on the dynamic behavior of the trap analyzed. Amongst other numerical methods the IIM-BEM is particularly well suited for this purpose, as it depicts the main physics (viscous flow, elastic deformation, electrostatics) that are relevant in DEP traps and many other micro-electromechanical-devices. More importantly, this technique is capable of dealing with both rigid and flexible boundaries, extending the use of quantitative simulation tools to a much wider class of devices than other techniques.

The authors are currently working on extensions of the method that will consider different viscosity ratios between the cell and the fluid buffer, as well as three-dimensional geometries.

Acknowledgements

The authors thank Professor K. M. Lim and Professor S. P. Lim at the Department of Mechanical Engineering, National University of Singapore, for many useful discussions and for making the computer cluster available for all the simulations in this paper.

Notes and references

- 1 J. P. Desai, A. Pillarisetti and A. D. Brooks, *Annu. Rev. Biomed. Eng.*, 2007, **9**, 35–53.
- 2 E. G. Cen, C. Dalton, Y. Li, S. Adamia, L. M. Pilarski and K. V. I. S. Kaler, *J. Microbiol. Methods*, 2004, **58**, 387–401.
- 3 R. Holzel and F. F. Bier, *IEE Proc. Nanobiotechnol.*, 2003, **50**, 47–53.
- 4 M. Frenea, S. P. Faure, B. LePioufle, Ph. Coquet and H. Fujita, *Mater. Sci. Eng., C*, 2003, **23**, 597–603.
- 5 J. Voldman, M. Toner, M. L. Gray and M. A. Schmidt, *J. Electrostat.*, 2003, **57**, 69–90.
- 6 S. Fiedler, S. G. Shirley, T. Schnelle and G. Fuhr, *Anal. Chem.*, 1998, **70**, 1909–1915.
- 7 Y. Li and K. V. I. S. Kaler, *Anal. Chim. Acta*, 2004, **507**, 151–161.
- 8 K. L. Chan, H. Morgan, E. Morgan, I. T. Cameron and M. R. Thomas, *Biochim. Biophys. Acta*, 2000, **1500**, 313–322.
- 9 M. P. Hughes, H. Morgan and F. J. Rixon, *Eur. Biophys. J.*, 2001, **30**, 268–272.
- 10 T. B. Jones, *IEEE Eng. Med. Biol. Mag.*, 2003, **22**(6), 33–42.
- 11 H. Pohl, *Dielectrophoresis*, Cambridge University Press, Cambridge UK, 1978.
- 12 J. Suehiro and R. Pethig, *J. Phys. D: Appl. Phys.*, 1998, **31**, 3298–3305.
- 13 A. Rosenthal, B. M. Taff and J. Voldman, *Lab Chip*, 2006, **6**, 508–515.
- 14 D. V. Le, B. C. Khoo and J. Peraire, *J. Comput. Phys.*, 2006, **220**, 109–138.
- 15 C. Rosales and K. M. Lim, *Electrophoresis*, 2005, **26**, 2057–2065.
- 16 X. Wang, X.-B. Wang and P. R. C. Gascoyne, *J. Electrostat.*, 1997, **39**, 277–295.
- 17 C. A. Brebbia and R. Butterfield, *Appl. Math. Model.*, 1978, **2**, 132–134.
- 18 D. Beatovic, *A Galerkin formulation of the boundary element method for two and three dimensional problems in electrostatics*, PhD thesis, Worcester Polytechnic institute, Worcester, MA, USA, 1992.
- 19 R. Barrett, M. Berry, T. F. Chan, J. Demmel, J. Donato, J. Dongarra, V. Eijkhout, R. Pozo, C. Romine and H. Van der Vorst, *Templates for the Solution of Linear Systems: Building Blocks for Iterative Methods*, SIAM, Philadelphia, PA, USA, 1994.
- 20 O. Axelsson, *Iterative Solution Methods*, Cambridge University Press, Cambridge, UK, 1994.
- 21 R. J. LeVeque and Z. Li, *SIAM J. Numer. Anal.*, 1994, **31**, 1019–1044.
- 22 R. J. LeVeque and Z. Li, *SIAM J. Sci. Comput.*, 1997, **18**(3), 709–735.
- 23 L. Lee, *SIAM J. Sci. Comput.*, 2003, **25**(3), 832–856.
- 24 Z. Li and M. C. Lai, *J. Comput. Phys.*, 2001, **171**, 822–842.

-
- 25 D. V. Le, B. C. Khoo and J. Peraire, in *Proc. of the Third M.I.T. Conf. on Comput. Fluid and Solid Mech.*, Elsevier Science, June, 2005, pp. 710–716.
- 26 D. Calhoun, *J. Comput. Phys.*, 2002, **176**, 231–275.
- 5 27 Z. Li and C. Wang, *Commun. Math. Sci.*, 2003, **1**(1), 180–196.
- 28 D. Russell and Z. J. Wang, *J. Comput. Phys.*, 2003, **191**, 177–205.
- 29 J. Kim and P. Moin, *J. Comput. Phys.*, 1985, **59**, 308–323.
- 30 D. L. Brown, R. Cortez and M. L. Minion, *J. Comput. Phys.*, 2001, **168**, 464–499.
- 10 31 A. Wiegmann and K. P. Bube, *SIAM J. Numer. Anal.*, 2000, **37**(3), 827–862.
- 32 J. Adams, P. Swarztrauber, and R. Sweet, available on the web at <http://www.scd.ucar.edu/css/software/fishpack/>.
- 33 M. Dürr, J. Kentsch, T. Muller and M. Stelzle, *Electrophoresis*, 2003, **24**, 722–731. 15
- 34 A. Ramos, H. Morgan, N. G. Green and A. Castellanos, *J. Phys. D: Appl. Phys.*, 1998, **31**, 2338–2353.
- 35 C. Rosales, *Electrophoresis*, 2006, **27**, 1984–1995.
- 36 N. J. Petersen, R. P. H. Nikolajsen, K. B. Mogensen and J. P. Kutter, *Electrophoresis*, 2004, **25**, 253–269. 20
- 37 R. M. Hochmuth, *J. Biomech.*, 2000, **33**, 15–22.
- 38 J. P. Mills, M. Diez-Silva, D. J. Quinn, M. Dao, M. J. Lang, K. S. W. Tan, C. T. Lim, G. Milon, P. H. David, O. Mercereau-Puijalon, S. Bonnefoy and S. Suresh, *Proc. Natl. Acad. Sci. U. S. A.*, 2007, **104**, 9213–9217. 25

The Royal Society of Chemistry

Proofs for Correction

loc

Dear Author,

Paper No. b718153a

Please check the proofs of your paper carefully, paying particular attention to the numerical data, tables, figures and references.

When answering the queries below please ensure that any changes required are clearly marked **on the proof**. There is no need to e-mail your answers to the queries separately from the rest of your proof corrections.

Editor's queries are marked like this [Q1, Q2, ...], and for your convenience line numbers are indicated like this [5, 10, 15, ...].

Many thanks for your assistance.

Query	Remarks
Q1 For your information: You can cite this article before you receive notification of the page numbers by using the following format: (authors), (journal), (year), DOI: 10.1039/(paper number).	
Q2 Footnote 1: Is the text of the ESI footnote acceptable?	